Journal of Hazardous Materials 199–200 (2012) 170–178

Contents lists available at SciVerse ScienceDirect

Journal of Hazardous Materials

journal homepage: www.elsevier.com/locate/jhazmat

Assembly of CeO_2–TiO_2 nanoparticles prepared in room temperature ionic liquid on graphene nanosheets for photocatalytic degradation of pollutants

S. Ghasemi [a], S. Rahman Setayesh [a], A. Habibi-Yangjeh [b], M.R. Hormozi-Nezhad [a,c], M.R. Gholami [a,*]

[a] Department of Chemistry, Sharif University of Technology, P.O. Box 11365-9516, Tehran, Iran
[b] Department of Chemistry, Faculty of Science, University of Mohaghegh Ardabili, P.O. Box 179, Ardabil, Iran
[c] Institute for Nanoscience and Nanotechnology (INST), P.O. Box 14588-8969, Tehran, Iran

ARTICLE INFO

Article history:
Received 24 July 2011
Received in revised form 26 October 2011
Accepted 26 October 2011
Available online 2 November 2011

Keywords:
CeO_2–TiO_2 nanoparticles
CeO_2–TiO_2–graphene nanocomposites
Photocatalysis
Graphene
Room-temperature ionic liquid

ABSTRACT

CeO_2–TiO_2 nanoparticles were prepared by the sol–gel process using 2-hydroxylethylammonium formate as room-temperature ionic liquid and calcined at different temperatures (500–700 °C). CeO_2–TiO_2–graphene nanocomposites were prepared by hydrothermal reaction of graphene oxide with CeO_2–TiO_2 nanoparticles in aqueous solution of ethanol. The photocatalysts were characterized by X-ray diffraction, BET surface area, diffuse reflectance spectroscopy, scanning electron microscopy, and Fourier transformed infrared techniques. The results demonstrate that the room-temperature ionic liquid inhibits the anatase–rutile phase transformation. This effect was promoted by addition of CeO_2 to TiO_2. The addition of graphene to CeO_2–TiO_2 nanoparticles enhances electron transport and therefore impedes the charge recombination of excited TiO_2. The photodegradation results of the pollutants in aqueous medium under UV irradiation revealed that CeO_2–TiO_2–graphene nanocomposites exhibit much higher photocatalytic activity than CeO_2–TiO_2 and pure TiO_2. The photocatalytic activity of CeO_2–TiO_2–graphene nanocomposites decreases with additional increasing of the graphene content. Moreover, comparison of the photocatalytic activities of CeO_2–TiO_2–graphene with the other CeO_2–TiO_2–carbon demonstrates that CeO_2–TiO_2-graphene nanocomposites have the highest photocatalytic activity due to their unique structure and electronic properties. Chemical oxygen demand for solutions of the pollutants gave a good idea about mineralization of them.

1. Introduction

Herbicides and reactive dyes are the most important pollutants. 2,4-Dichlorophenoxyacetic acid (2,4-D) is one of the herbicides used in agriculture. The major route of 2,4-D contamination is run-off from agricultural field into natural water system [1]. Reactive Red 195 (RR195) is a known group of reactive dye used in textile industry. The release of these chemicals into the environment pollutes the ecosystem due to their toxicity and perturbation effects on aquatic life [2]. Photocatalysis is an advanced oxidation process which is used for photodegradation of various pollutants. Among various semiconductor photocatalysts, titanium dioxide (TiO_2) is the most suitable material for prevalent environmental applications [3]. However its wide band gap, high recombination rate of the generated charge carriers, and the slow transfer rate of electrons to oxygen limit the efficiency of this photocatalyst [4,5]. Recombination of electron–hole and photocatalytic activity of TiO_2 is strongly related to the size, surface area, crystallinity, and surface structure of that [4]. The performance of TiO_2 can be often enhanced by coupling of its particles with other semiconductor and incorporating electron-accepting materials, such as carbon nanostructures [4–6]. It has been reported that the addition of CeO_2 to TiO_2 improves its textural and structural properties [7]. The introducing of CeO_2 into TiO_2 framework not only improves the thermal stability of the ordered mesoporous structure but also effectively extends the photo-response of TiO_2 to the visible light region [8]. Cerium dioxide nanoparticles have been an attractive material due to their unique properties such as UV absorbing ability, high thermal stability, high electrical conductivity, large oxygen storage capacity, and the quick change of the oxidation state of cerium between Ce(III) and Ce(IV) [9]. TiO_2 and CeO_2 could produce a special electron transfer process which is able to facilitate the separation of the electron–hole pairs and thus improve activity of the photocatalyst [10]. Carbon is typically used as support for catalysts because of its high surface area [6]. Carbon nanostructures such as carbon nanotubes (CNTs) and graphene (GR) offer new opportunities to develop nanocomposites with unusual catalytic properties [11]. Presence of CNTs in TiO_2 matrix increases surface area of TiO_2 for trapping more organic pollutants, and increasing

* Corresponding author. Tel.: +98 2166165314; fax: +98 2166029165.
E-mail address: gholami@sharif.edu (M.R. Gholami).

0304-3894/$ – see front matter © 2011 Elsevier B.V. All rights reserved.
doi:10.1016/j.jhazmat.2011.10.080

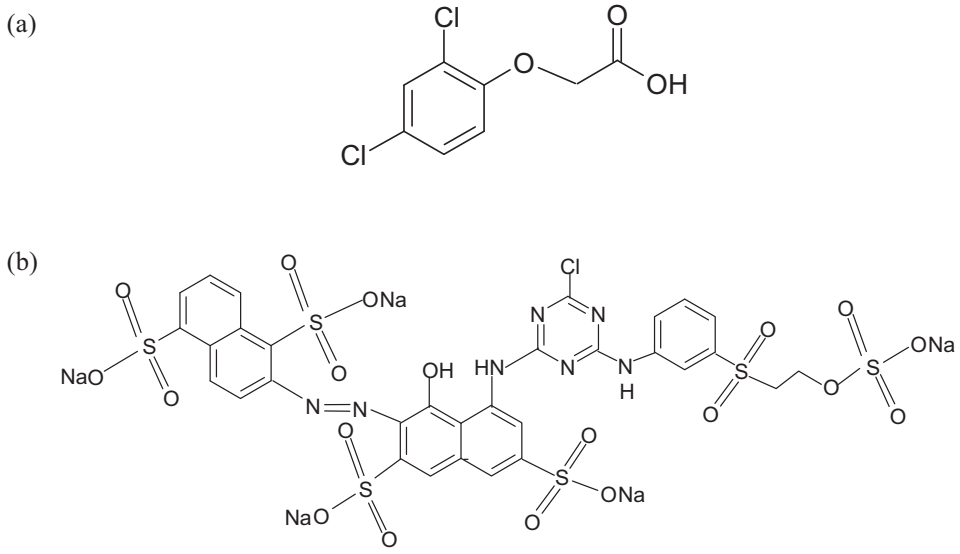

Fig. 1. Chemical structures of (a) 2,4-dichlorophenoxyacetic acid (2,4-D) and (b) Reactive Red 195 (RR195).

the rate of photocatalytic process [12]. In comparison with CNTs, GR is a two-dimensional sp^2-hybridized carbon nanosheet, which possesses many unique properties such as a zero band gap material, a very high mobility of charge carriers, and good mechanical strength [13–15]. Exfoliated GR sheets have theoretical surface areas of about 2600 $m^2\ g^{-1}$, making them highly desirable for using as a two-dimensional support of catalysts [16]. From the engineering point of view, GR has electronic and thermal properties, which may be comparable to those of single-walled carbon nanotubes with much lower production cost [14]. One of the possible ways to utilize these properties is to incorporate GR sheets in a composite material. GR containing composite materials have recently been attracting much attention [17]. The combination of TiO_2 with GR will surely develop the photocatalytic property of TiO_2 [13]. In this work, CeO_2–TiO_2 (CT) nanoparticles were prepared by the sol-gel method using a room-temperature ionic liquid (RTIL), 2-hydroxylethylammonium formate, as a solvent. The RTIL could assist in reducing gel shrinkage during sol ageing and drying, which prevents the collapse of pore structure, and the loss of surface area. CeO_2–TiO_2–graphene (CT–GR) nanocomposites were prepared by hydrothermal reaction of graphene oxide (GO) and CT nanoparticles in aqueous solution of ethanol. The samples were characterized by different techniques. The photocatalytic activities were examined by degradation of RR195 and 2,4-D pollutants.

2. Experimental

2.1. Reagents

Tetraisopropylorthotitanate, $Ce(NO_3)_3{\cdot}6H_2O$, sulfuric acid (98%), $K_2S_2O_8$, P_2O_5, hydrochloride acid, sodium hydroxide, 2-aminoethanol, formic acid, acetonitrile, ethanol, 2,4-dichlorophenoxyacetic acid (2,4-D, Mw = 221.04 g mol^{-1}) were purchased from Merck. Graphite powder was purchased from Fluka. Reactive Red 195 (RR195, Mw = 1136.32 g mol^{-1}, C.I. = 93050-79-4) textile dye was provided by Color Research Center of Iran. The chemical structures of 2,4-D and RR195 are shown in Fig. 1.

2.2. Synthesis of GO

GO was synthesized by using the modified Hummers' method. 3.00 g of graphite powder was added into a mixture of 12 mL of concentrated H_2SO_4, 2.50 g of $K_2S_2O_8$, and 2.50 g of P_2O_5. The mixture was heated to 80 °C and stirred for 5 h in an oil bath. The suspension was diluted with 500 mL of deionized water. The product was obtained by filtering the solution using 0.2 μm Nylon film, washed with deionized water several times and dried under ambient condition. The oxidized graphite was added to the 460 mL of H_2SO_4 in an ice bath. Then, 60 g of $KMnO_4$ was put slowly with controlling the temperature below 10 °C. Stirring was continued for 2 h at 35 °C. After that 920 mL of deionized water was added slowly with keeping the temperature below 50 °C. After 2 h, 2.8 L of deionized water and 50 mL of 30% H_2O_2 were added to the mixture. The mixture was centrifuged and washed with a total of 5 L of 10% HCl solution followed by 5 L of deionized water to remove the acid. The resulting solid was subjected to dialysis for a week. Finally, the product was dried under the vacuum at ambient temperature [18].

2.3. Synthesis of CeO_2–TiO_2 nanoparticles using RTIL

Nanocrystalline CeO_2–TiO_2 was synthesized by the sol–gel process using 2-hydroxylethylammonium formate as an RTIL. 2-Hydroxylethylammonium formate was prepared by placing 2-aminoethanol in a two-necked flask equipped with a reflux condenser and a dropping funnel. The flask was mounted in an ice bath. Under vigorous stirring with a magnetic bar, formic acid was added drop wise to the flask about 45 min. Stirring was continued for 24 h at room temperature to obtain a viscous clear liquid [2]. The reaction for preparation of the RTIL can be written as follows:

(1)

4.00 g of Tetraisopropylorthotitanate (Tipt) was added to the first part of ethanol (12 mL) under vigorous stirring. After 10 min, 1.00 g of 2-hydroxylethylammonium formate was put in. The transparent solution was formed following addition of the RTIL. The solution was stirred for 2 h and then the second part of ethanol (12 mL) with the desired amount of Ce $(NO_3)_3{\cdot}6H_2O$ (2.5, 5, 10, 15 and 20 wt%) was added. The final solution was stirred for another 2 h. Finally, the metal doped TiO_2 products were dried for 12 h at

100 °C and calcined for 4 h at various temperatures (500–700 °C) under nitrogen atmosphere.

2.4. Synthesis of CeO_2–TiO_2–graphene nanocomposite

CeO_2–TiO_2–graphene (CT–GR) nanocomposites were synthesized by hydrothermal method based on Zhang's work with some modifications [19]. 2.00 mg of GO was dispersed in deionized water (20 mL) and ethanol (10 mL) by ultrasonic treatment for 1 h. Then 0.2 g of the CT nanoparticles calcined at 650 °C was added to this solution and stirred for another 2 h to get a homogeneous suspension. The suspension was placed in a 80 mL Teflon-sealed autoclave and heated at 120 °C for 24 h for reducing GO to graphene and depositing of CT nanoparticles on carbon substrate. Finally, the resulting nanocomposite was recovered by filtration, washed with deionized water several times and dried at room temperature. For comparison, CT–activated carbon and CT–CNTs (with the same content of carbon) were prepared with the same method used for preparation of CeO_2–TiO_2–graphene nanocomposite.

2.5. Characterization of the prepared samples

The X-ray diffraction (XRD) patterns were obtained on a D4 X-ray diffractometer using Cu K_α radiation ($\lambda = 0.15406$ nm) as the X-ray source. The specific surface area of the products was calculated from the nitrogen adsorption/desorption isotherms at 77 K, using Belsorp apparatus. All of the samples were degassed under N_2 for 4 h at 100 °C prior to measurement. The Fourier transformed infrared (FT-IR) spectrum was recorded in the transmission mode on ABB BOMER MB series spectrophotometer. The dried samples of CT or CT–GR particles were grounded with KBr and the mixture was compressed into a pellet. The spectrum was taken from 4000 to 400 cm^{-1}. Diffuse reflectance spectroscopy (DRS) of the samples was performed using a Cintra 40 instrument with $BaSO_4$. Morphology of the photocatalysts was characterized using scanning electron microscopy (SEM) (Philips XN 30).

2.6. Photocatalysis experiments

Photocatalysis experiments were carried out in a pyrex reactor. The UV source was provided by OSRAM 125 W high-pressure mercury lamp placed above the reactor as demonstrated in Fig. 2. Reactor and UV source were surrounded by a circulating water jacket to maintain constant temperature.

The pollutant solutions (100 mL, 20 ppm) and the photocatalysts (80 ppm for RR195 and 200 ppm for 2,4-D) were fed into the reactor and the pH was adjusted using phosphate buffer. Prior to irradiation, the suspension was magnetically stirred for 30 min in dark to favor the adsorption–desorption equilibrium. After dark

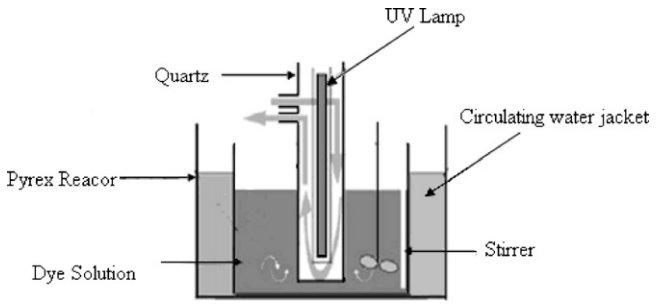

Fig. 2. Scheme for photocatalysis experiments.

adsorption, the lamp was switched on to initiate the photocatalytic reactions. Samples (*ca.* 2 mL) were withdrawn for UV–vis analysis at regular time intervals and centrifuged for 10 min at the rate of 15,000 rpm. The concentration of RR195 and 2,4-D in each degraded sample was determined spectrophotometrically (by GBC Cintra 40) at $\lambda = 542$ and 283 nm, respectively. The conditions for degradation of the pollutants have been found to be [pollutant] = 20 ppm, [catalyst] = 200 ppm and pH = neutral. The extent of degradation of the pollutants was also followed by COD measurements by titration of the pollutants solutions with $KMnO_4$ solution at regular time intervals.

3. Results and discussion

3.1. Characterization of the photocatalysts

3.1.1. UV–vis absorption spectra of GO and CT–GR

The UV–vis absorption spectrum of GO (Fig. 3) shows a peak at about 233 nm which is due to $\pi \rightarrow \pi^*$ transitions of aromatic C=C bonds, and a shoulder at about 290–300 nm, corresponding to $n \rightarrow \pi^*$ transition of the C=O bond [20]. After hydrothermal reduction treatment at 120 °C for 24 h the absorption peak of GO at 233 nm red-shifts to higher wavelength and the shoulder disappeared (Fig. 3b). This is accompanied by the change of GO solution color from yellow brown to black which confirms the reduction of GO to GR by CT nanoparticles [21].

3.1.2. X-ray diffraction analysis

The XRD patterns of CT nanoparticles calcined at different temperatures are demonstrated in Fig. 4. At 500 °C, only the anatase peaks ($2\theta = 25.20°$, 37.76°, 47.92°, and 53.78°) were detected which means TiO_2 exists as anatase structure [22]. By further increasing of annealing temperature (up to 700 °C), rutile phase was formed. No cerium oxide crystalline phases are detected, suggesting that CeO_2 could be well dispersed over the titania surface [23] or the probable insertion of some Ce^{4+} in the titania network or the particles are

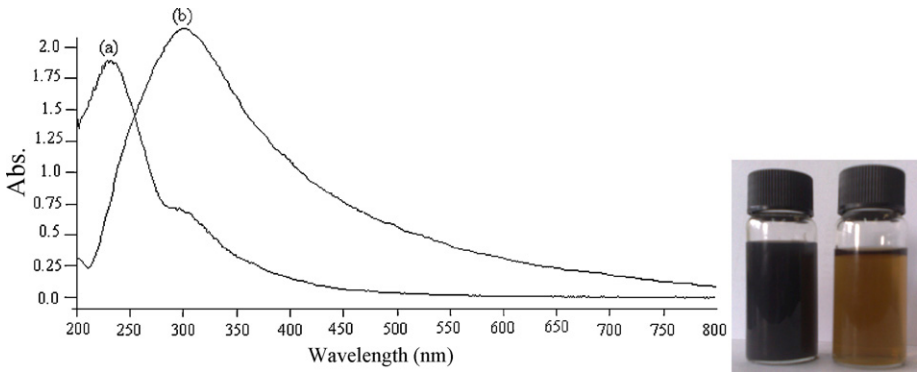

Fig. 3. UV–vis absorption spectra of (a) GO and (b) CT–GR nanocomposite.

Table 1
Textural property of the TiO_2, CT and CT–carbon (AC, CNTs, and GR) nanoparticles synthesized with the RTIL and calcined at 650 °C.

Photocatalyst	BET surface area ($m^2\ g^{-1}$)	Mean pore diameter (nm)	Total pore volume ($cm^3\ g^{-1}$)	E_g (eV)	Particle size (nm)
TiO_2 (without RTIL)	14.88	8.90	0.0330	3.30	122
TiO_2 (with RTIL)	44.02	8.71	0.0960	3.10	85
CeO_2–TiO_2/RTIL	174.84	6.89	0.3012	2.70	48
CeO_2–TiO_2–AC	257.43	3.32	0.2139	2.56	36
CeO_2–TiO_2–CNTs	277.94	3.97	0.2756	2.26	28
CeO_2–TiO_2–GR	334.64	3.70	0.3096	2.07	25

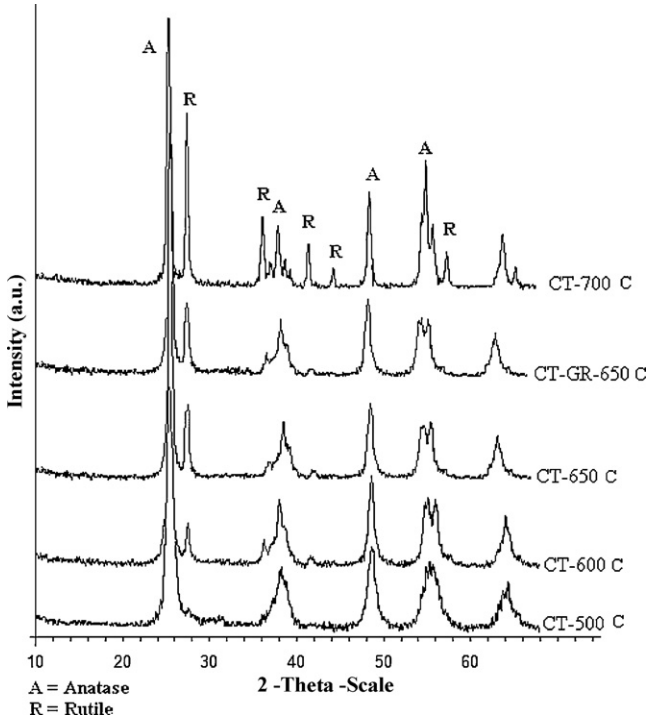

Fig. 4. XRD patterns of CT–GR nanoparticles calcined at 650 °C and CT nanoparticles prepared in the RTIL and calcined at various temperatures.

too small to be detected by XRD [24]. The XRD patterns of CT–GR nanocomposites that CT was calcined in 650 °C are also shown in Fig. 4. CT–GR nanocomposites exhibits XRD pattern similar to CT. Notably, no diffraction peaks belonging to the pure GR are observed in the XRD pattern of the nanocomposite. The characteristic peak of GR at 24.5° might be shielded by the main peak of anatase TiO_2 at 25.4° [25]. It is interesting to note that, preparation of TiO_2 in the RTIL and the addition of CeO_2 have noticeable effect on the XRD pattern of the TiO_2 calcined at 700 °C (Fig. 5). As it can be seen in Fig. 5,

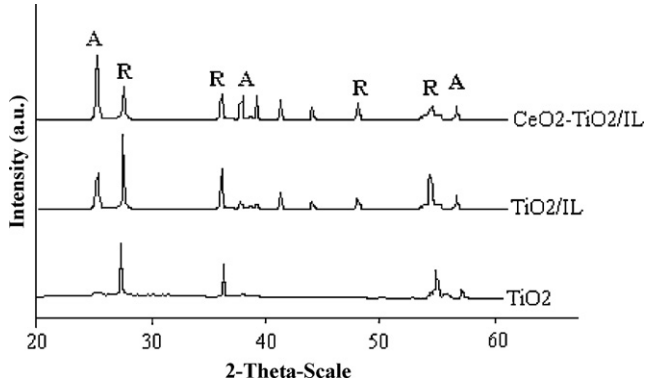

Fig. 5. Effect of the RTIL and CeO_2 on XRD pattern of TiO_2 nanoparticles calcined at 700 °C.

the TiO_2 prepared without the RTIL has only rutile phase, while the one prepared in the RTIL still possessed anatase phase. Moreover, the percentage of anatase phase increased more in the presence of CeO_2.The increase of anatase phase means that preparation in the RTIL and addition of CeO_2 retarded the anatase–rutile transformation. The average crystal size for samples calcined at 650 °C was calculated by applying the Scherrer's formula on the anatase diffraction peaks [26] (Table 1):

$$D = \frac{0.89\lambda}{\beta \cos\theta} \quad (2)$$

where D is the crystallite size, λ is the wavelength of incident ray, β is the full width at half-maximum of the peak, and θ is the position of the plane peak. The results revealed that the incorporation of CeO_2 and preparation in the RTIL decreases the crystalline size due to the prevention of coagulation of particles during heat treatment process and the reduction of gel shrinkage during sol ageing and gel drying [2].

3.1.3. BET surface area

Effect of the RTIL, Ce, and carbon source on surface area, mean pore diameter and total pore volume of TiO_2 nanoparticles calcined at 650 °C are presented in Table 1. The surface area of TiO_2 prepared in the RTIL ($44.02\ m^2\ g^{-1}$) was higher than the one prepared without the RTIL ($14.88\ m^2\ g^{-1}$). The RTIL could assist in reducing gel shrinkage during sol ageing and gel drying, which could prevent the collapse of the pore structure. The surface area also increased by addition of CeO_2 to TiO_2 ($174.84\ m^2\ g^{-1}$). This addition stabilized textural structure, hindering agglomeration, and thus reducing the extent of surface area loss during calcination [14]. Since GR sheets have high surface area, CT–GR nanocomposites would have higher surface area than CT–AC and CT–CNTs nanocomposites. During reduction of GO, GR sheets can easily aggregate due to the removal of oxygenate groups. Therefore, the decoration of both sides of GR with TiO_2 nanoparticles is an effective approach for depressing the aggregation of GR sheets, leading to the high BET surface area for CT–GR nanocomposites [27].

3.1.4. SEM images

SEM images of the samples are shown in Fig. 6. It is obvious that CeO_2–TiO_2 nanoparticles prepared in the RTIL are significantly smaller than pure TiO_2. The SEM images also show that CT nanoparticles are distributed well on the surface of carbon source.

3.1.5. FT-IR analysis

Fig. 7 represents the FT-IR spectra of TiO_2, CT calcined at 650 °C and CT–GR prepared by hydrothermal method. The bands around $3400\ cm^{-1}$ belong to O–H stretching, which means that TiO_2 nanoparticles easily adsorb water in the air [28]. The broad band at low frequency (below $1000\ cm^{-1}$) was attributed to Ti–O–Ti stretching vibration. The IR spectrum of CT does not show any band corresponding to Ce–O. It may be due to the low content of incorporated Ce; therefore the intensity of the band related to Ce–O–Ti is very low. In addition, the bending frequency of Ce–O might be overlapped with Ti–O bending frequency, below $1000\ cm^{-1}$, and therefore the overlap peaks is observed in this region. The

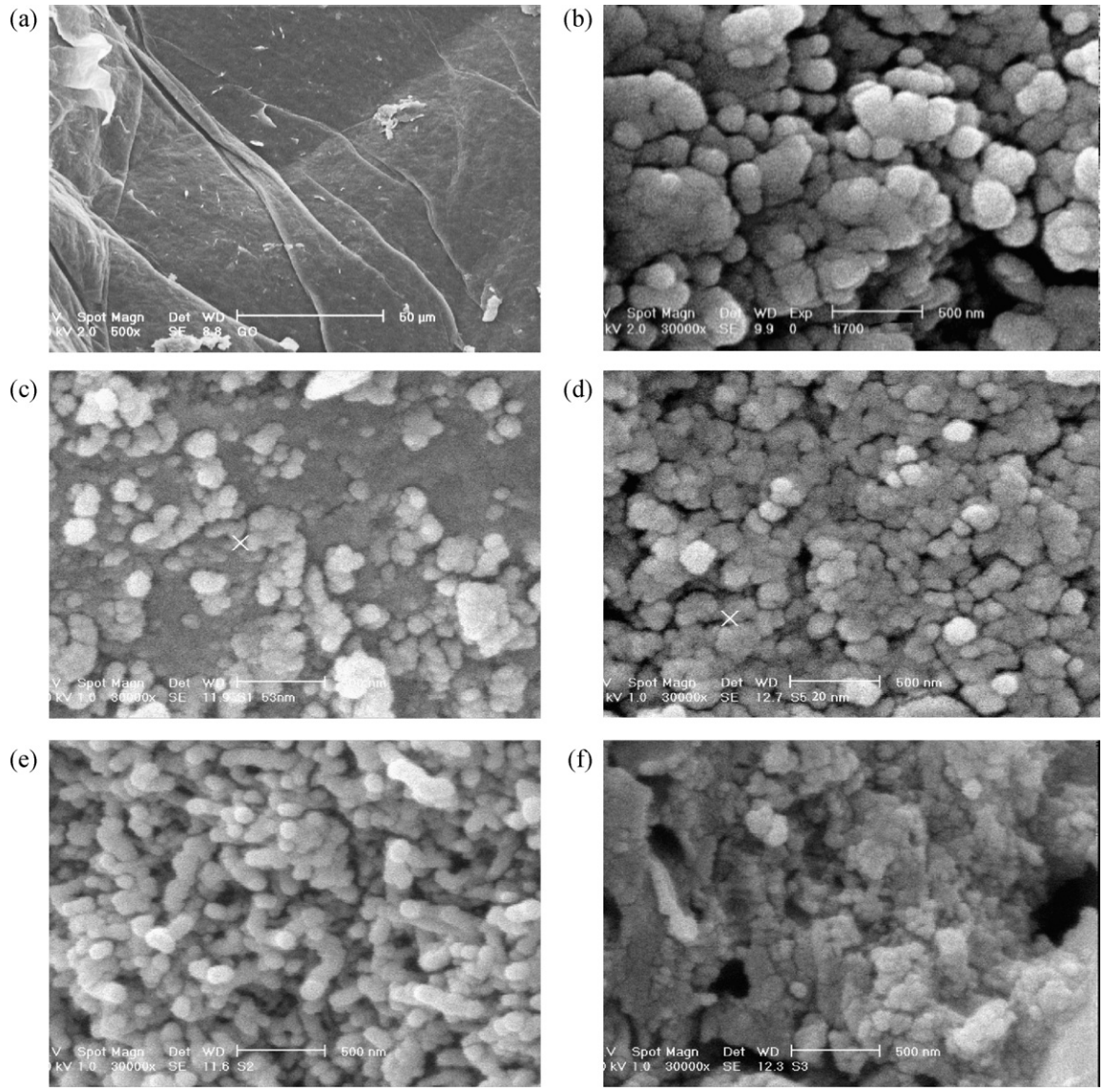

Fig. 6. SEM images of (a) GO sheet, (b) TiO_2 nanoparticles prepared in the RTIL, (c) CT nanoparticles, (d) CT–GR, (e) CT–CNTs and (f) CT–AC nanocomposites calcined at 650 °C (the scale bars in the figures represent 500 nm).

absorption band appearing at 1600 cm^{-1} in CT–GR composites clearly showed the skeletal vibration of the graphene sheets, which confirms the reduction of GO to GR during the hydrothermal reaction [19,29].

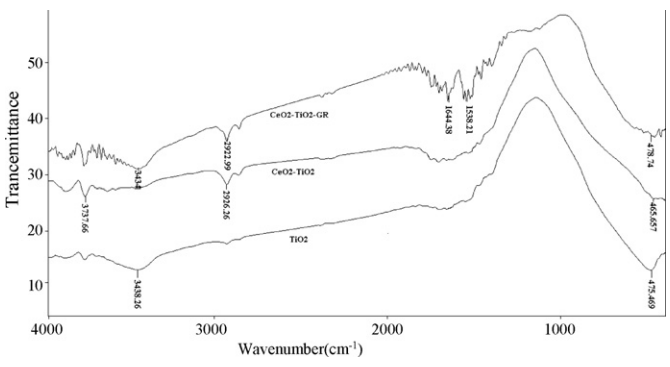

Fig. 7. The FT-IR spectra for TiO_2, CT and CT–GR calcined at 650 °C.

3.1.6. DRS analysis

The effect of CeO_2 and carbon source on the band structure and band gap energy of TiO_2 nanoparticles is shown by DRS spectra (Fig. 8). Characteristic band for titanium dioxide appeared at about

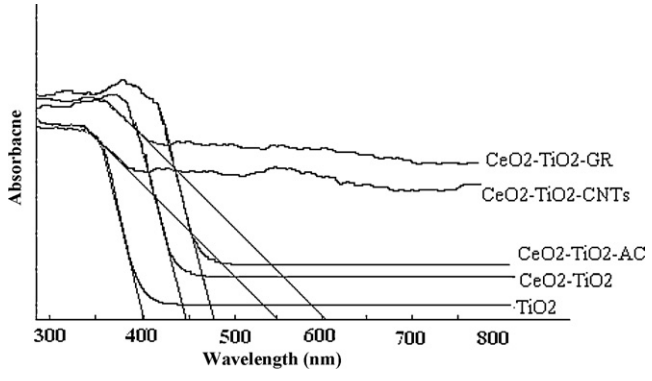

Fig. 8. Diffuse reflectance spectra of TiO_2 and CeO_2–TiO_2 nanoparticles and CeO_2–TiO_2–carbon nanocomposites calcined at 650 °C.

370 nm. This absorption is associated to the $O^{2-} \rightarrow Ti^{4+}$ charge-transfer, related to electron excitation from the valence band to the conduction band [4]. Red shift to the visible light region is detected for CT nanoparticles. This result revealed that Ce cations might be incorporated into the lattice of TiO_2. A red shift to higher wavelength in the absorption edge of CT–GR nanocomposites has also been observed. Comparison with CT, for CT–carbon a broad background absorption in the visible light region is observed. This can be attributed to the formation of Ti–O–C chemical bond in the prepared nanocomposites [19,29].

3.2. The factors influencing on the photocatalytic activities

The efficiency of the degradation reaction was calculated from the following equation:

$$X\% = \frac{(C_0 - C)}{C_0} \times 100 \quad (3)$$

where X is the efficiency of degradation, C_0 is the initial concentration and C is concentration of RR195 or 2,4-D after degradation.

The photocatalytic degradation of the pollutants follows the first-order decay kinetics. Studies showed that the photocatalytic degradation rate of the pollutants in heterogeneous photocatalytic oxidation systems under UV-light illumination obeyed Langmuir–Hinshelwood (L–H) kinetics model (Eq. (4)) [29].

$$r = -\frac{dC}{dt} = \frac{kKC}{1 + KC} \quad (4)$$

where r, C, t, k, K are the oxidation rate ($mg\,L^{-1}\,min^{-1}$), the concentration of the pollutant ($mg\,L^{-1}$), the illumination time (min), the reaction rate constant (min^{-1}), and the adsorption coefficient of the pollutant on the photocatalyst ($L\,mg^{-1}$), respectively.

At low initial concentration of the pollutant, the reaction rate is proportional to the pollutant concentration and the reaction is pseudo-first order. So Eq. (4) can be changed to Eq. (5).

$$\ln\left(\frac{C_0}{C}\right) = kKt = k_{app}t \quad (5)$$

The apparent rate constant (k_{app}) for the degradation of the pollutant can be calculated by plotting $\ln(C_0/C)$ versus t.

3.2.1. Effect of calcinations temperature on the photocatalytic activity of CT nanoparticles

Effect of calcinations temperature on the photocatalytic activity of CT nanoparticles prepared in the RTIL is presented in Fig. 9. At 500 °C, the nanoparticles have the lowest photocatalytic activity, because the anatase phase is dominated. The highest rate constant is obtained when CT nanoparticles is calcined at 650 °C. Therefore, the catalyst calcined at 650 °C was chosen for other

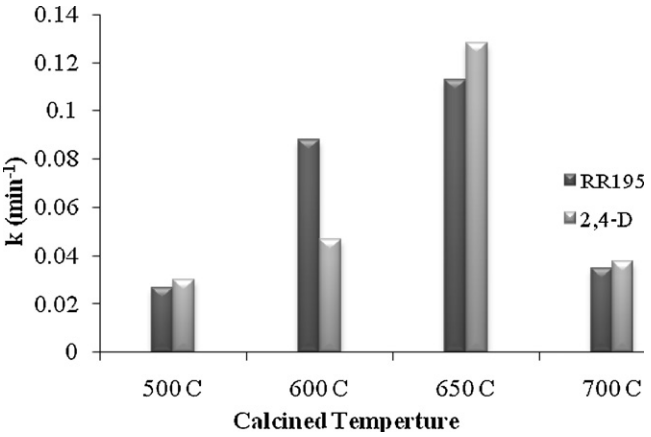

Fig. 9. Effect of calcination temperature on the photocatalytic activity of CT nanoparticles prepared in the RTIL (2.5% CeO_2–TiO_2).

experiments. However the photocatalytic activity decreases with increasing calcination temperature. It has been reported that the high-performance photocatalyst consists of a mixture of anatase and rutile phases with a high fraction of anatase. The transfer of an electron between the crystal phases can reduce electron–hole recombination in the electron-donor phase [2]. At high calcinations temperature, the photocatalyst loses the active surface area because of sintering and crystalline growth, and therefore the photocatalytic activity decreases. The RTIL and CeO_2 play a key role here. The former retarded phase transformation, which anatase still exists at higher temperatures. The latter contributes to this retardation, stabilizing the nanoparticles and a good crystallinity obtains with increasing calcinations temperature [30].

3.2.2. Effect of the amount of CeO_2 loading

Effect of the amount of Ce loading on the photocatalytic activity of CT nanoparticles is demonstrated in Fig. 10. The photocatalytic activity of TiO_2 nanoparticles was enhanced by the addition of CeO_2. Cerium oxide has multi functional role. It traps electrons, which retarded electron-hole recombination and increasing $O_2^{\bullet -}$ for degradation of the pollutants by the 6–10 equations:

$$TiO_2 + h\nu \rightarrow e^-_{CB} + h^+_{VB} \quad (6)$$

$$Ce^{4+} + e^-_{CB} \rightarrow Ce^{3+} \quad (7)$$

$$Ce^{3+} + O_2 \rightarrow Ce^{4+} + O_2^{\bullet -} \quad (8)$$

$$O_2^{\bullet -} + 4H^+ \rightarrow 2^{\bullet}OH \quad (9)$$

$$\text{pollutant} + {}^{\bullet}OH \rightarrow \text{degradation products} \quad (10)$$

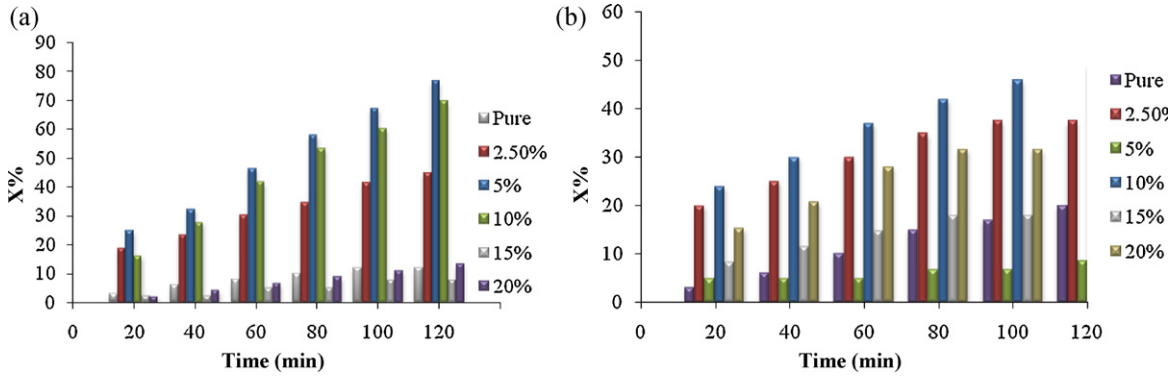

Fig. 10. Effect of Ce loading on the photocatalytic activity of CT nanoparticles calcined at 650 °C for degradation of (a) RR195 and (b) 2,4-D.

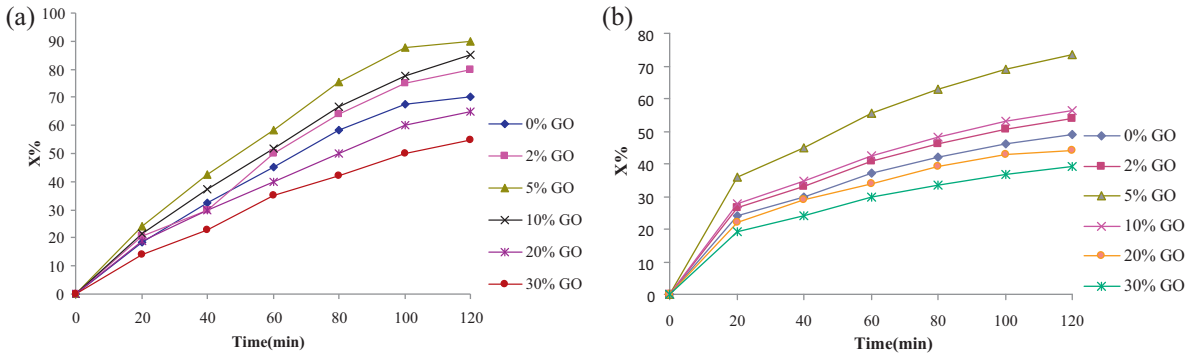

Fig. 11. Effect of GO loading on the photocatalytic activity of CT nanoparticles calcined at 650 °C for degradation of (a) RR195 and (b) 2,4-D.

The results indicated that the photocatalytic activities increases with increasing the amount of cerium dopant until a maximum is reached at 5 wt% for RR195 and 10 wt% for 2,4-D. This behavior might be associated with the separation of photoinduced electron–hole pairs. Further increasing in cerium content up to 20 wt% leads to a decline in the catalytic activity. As the concentration of CeO_2 phase increases, the impurity band would become broader and thus the charge separation gap became narrower and the recombination of electron–hole pairs would be rapid. There are two factors which limited the amount of Ce loading: (i) blockage of active sites by excess amounts of Ce introduced in the photocatalysts and (ii) an increase in opacity and light scattering of CeO_2–TiO_2 nanoparticles at a high concentration leads to a decrease in the passage of irradiation through the sample [31,32]. The greater concentration of Ce loading for 2,4-D degradation than the case for degradation of RR195 suggests that 2,4-D is more difficult for the photocatalytic degradation, which could be due to its more stable and inert chemical structure.

3.2.3. *Effect of the amount of GO loading*

The photocatalytic degradation of RR195 and 2,4-D over CT–GR nanocomposites are shown in Fig. 11. The degradation of RR195 and 2,4-D increases with increasing the amount of GO content and reaches maximum at 5%. Further increasing GO content to 30% leads to a decrease in degradation of the pollutants. The enhancement of the photocatalytic activity for degradation could be attributed to the excellent electric conductivity and large specific surface area of CT–GR nanocomposites. The photogenerated electrons transport to the surface of the nanocomposites more easily, thus the recombination between photoinduced electrons and holes are inhibited [33]. Decrease of the photocatalytic activity with higher GO content may be due to the fact that the opportunity for the collision of electrons and holes increases, therefore the recombination of the photo-generated electron–hole pairs is promoted. Increasing GO ratio also lowers the contact surface of TiO_2 nanoparticles with the illuminated light [34].

3.2.4. *Comparison of the photocatalytic activities of CT–GR with CT–CNTs and CT–AC nanocomposites*

The photocatalytic activity and chemical oxygen demand (COD) removal of the prepared TiO_2, CT, CT–GR, CT–CNTs, and CT–AC nanocomposites are shown in Figs. 12 and 13. It is clear from Fig. 12 that CT–carbon nanocomposites show significant increase in the photodegradation of RR195 and 2,4-D compared to CT. The high surface area for carbon sources allows dispersion of CT nanoparticles. The nanocomposites also have a high propensity for trapping or adsorbance of reactants, and facilitate transfer of the pollutants to active sites [35]. Among the prepared photocatalysts, CT–GR nanocomposite shows the highest photocatalytic activity and COD removal. Then, GR sheets can be good supports for deposition of CT nanoparticles [36]. GR has large specific surface area and strong capacity of adsorption, therefore enhances adsorption ability of CT–GR nanocomposite for the pollutants. Moreover, it can act as electron acceptor due to its two dimensional π-conjugation structure. The excited electrons of CT nanoparticles can quickly transfer from the conduction band of CT to GR (Fig. 13b). Thus, the recombination of photo-generated charge carriers is reduced and more reactive species will be existed for the photodegradation of the pollutants [37].

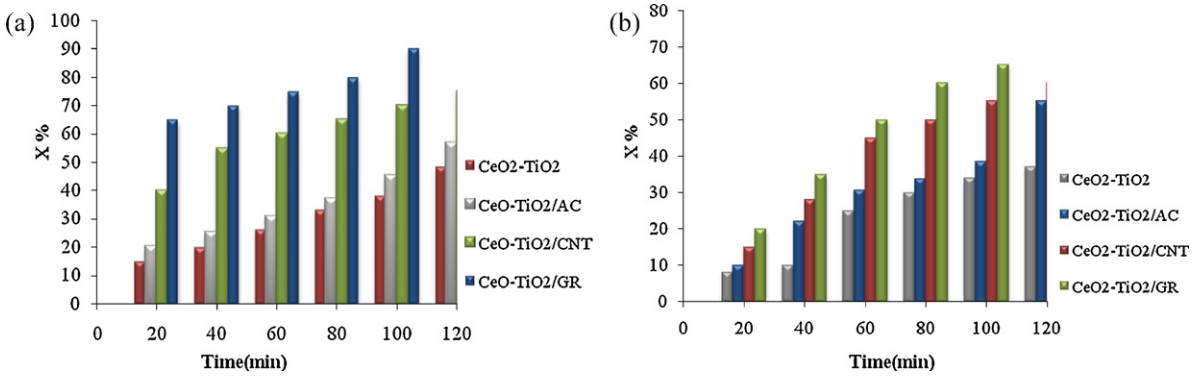

Fig. 12. The photocatalytic activity of TiO_2, CT, CT–GR, CT–CNT and CT–AC calcined at 650 °C for degradation of (a) RR195 and (b) 2,4-D.

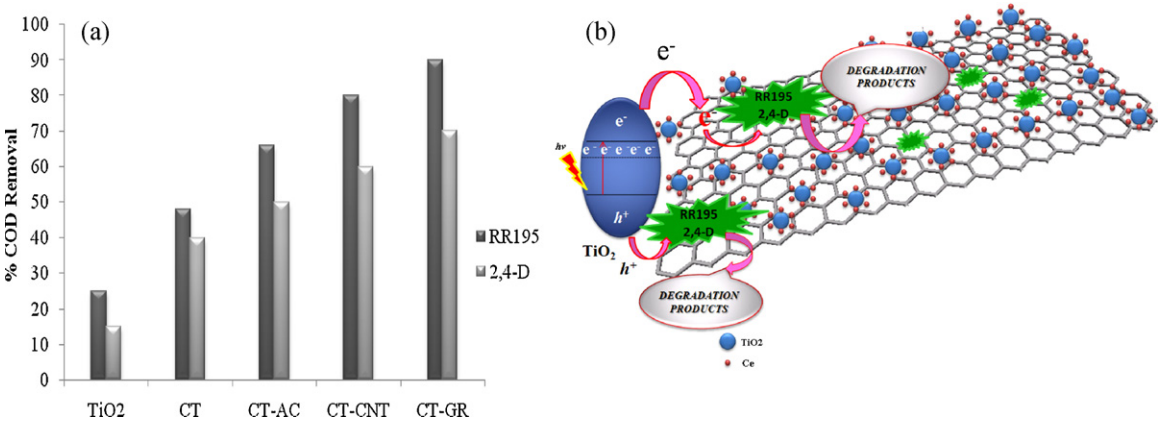

Fig. 13. (a) COD removal of the pollutants solutions on TiO_2, CT, CT–GR, CT–CNT and CT–AC nanoparticles calcined at 650 °C. (b) Schematic structure of CT–GR nanocomposite and tentative processes of the photodegradation of the pollutants.

4. Conclusions

TiO_2 and CeO_2–TiO_2 (CT) nanoparticles and CeO_2–TiO_2–carbon nanotubes (CT–CNTs), CeO_2–TiO_2–activated carbon (CT–AC) and CeO_2–TiO_2–graphene (CT–GR) nanocomposites were prepared and characterized by various techniques. The results revealed that the incorporation of CeO_2 in TiO_2 and preparation in the RTIL decreased the crystalline size, increased the surface area and retarded anatase–rutile phase transformation. Red shifts to the visible light region are detected for CT nanoparticles and CT–GR nanocomposites. Photocatalytic activities of the photocatalysts were investigated by degradation of two selected pollutants (Reactive Red 195 and 2,4-dichlorophenoxyacetic acid) in water. CT nanoparticles calcined at 650 °C have the highest photocatalytic activity. Moreover, the photocatalytic activities increases with the amount of cerium cations until maxima are reached at 5% for RR195 and 10% for 2,4-D. CT–carbon nanocomposites demonstrate significant increase in the photodegradation of RR195 and 2,4-D compared to CT. Among CT–carbon nanocomposites, CT–GR nanocomposite shows highest phtocatalytic activity and COD removal. The increase in photocatalytic activity can be attributed to higher surface area, and lower electron-hole recombination rate.

Acknowledgement

The authors are grateful to the Sharif University of Technology for financial support.

References

[1] L. Jianfa, M. Jiang, W. Huan, L. Yimin, Addition of modified bentonites in polymer gel formulation of 2,4-D for its controlled release in water and soil, J. Agric. Food Chem. 57 (2009) 2868–2874.
[2] S. Ghasemi, S. Rahimnejad, S. Rahman Setayesh, M. Hosseini, M.R. Gholami, Kinetics investigation of the photocatalytic degradation of Acid Blue 92 in aqueous solution using nanocrystalline TiO_2 prepared in an ionic liquid, Prog. React. Kinet. Mech. 34 (2009) 55–76.
[3] J. Du, X. Lai, N. Yang, J. Zhai, D. Kisailus, F. Su, D. Wang, Hierarchically ordered macro-mesoporous TiO_2-graphene composite films: Improved mass transfer, reduced charge recombination, and their enhanced photocatalytic activities, ACS Nano 5 (2011) 590–596.
[4] S. Ghasemi, S. Rahimnejad, S. Rahman Setayesh, S. Rohani, M.R. Gholami, Transition metal ions effect on the properties and photocatalytic activity of nanocrystalline TiO_2 prepared in an ionic liquid, J. Hazard. Mater. 172 (2009) 1573–1578.
[5] M. Maicu, M.C. Hidalgo, G. Colón, J.A. Navio, Comparative study of the photodeposition of Pt, Au and Pd on pre-sulphated TiO_2 for the photocatalytic decomposition of phenol, J. Photochem. Photobiol. A: Chem. 217 (2011) 275–283.
[6] M. Tian, M. Malig, S. Chen, A. Chen, Synthesis and electrochemical study of TiO_2-supported PdAu nanoparticles, Electrochem. Commun. 13 (2011) 370–373.
[7] D.H. Yoo, T.V. Cuong, V.H. Pham, J.S. Chung, N.T. Khoa, E.J. Kim, S.H. Hahn, Enhanced photocatalytic activity of graphene oxide decorated on TiO_2 films under UV and visible irradiation, Curr. Appl. Phys. 11 (2011) 805–808.
[8] B. Jiang, S. Zhang, X. Guo, B. Jin, Y. Tian, Preparation and photocatalytic activity of CeO_2/TiO_2 interface composite film, Appl. Surf. Sci. 255 (2009) 5975–5978.
[9] E.K. Goharshadi, S. Samiee, P. Nancarrow, Fabrication of cerium oxide nanoparticles: characterization and optical properties, J. Colloid Interface Sci. 356 (2011) 473–480.
[10] T. Cao, Y. Li, C. Wang, L. Wei, C. Shao, Y. Liu, Three-dimensional hierarchical CeO_2 nanowalls/TiO_2 nanofibers heterostructure and its high photocatalytic performance, J. Sol-Gel Sci. Technol. 55 (2010) 105–110.
[11] G. Williams, B. Seger, P.V. Kamat, TiO_2-graphene nanocomposites, UV-assisted photocatalytic reduction of graphene oxide, ACS Nano 2 (2008) 1487–1491.
[12] H.R. Jafry, M.V. Liga, Q. Li, A.R. Barro, Single walled carbon nanotubes (SWNTs) as templates for the growth of TiO_2: the effect of silicon in coverage and the positive and negative synergies for the photocatalytic degradation of Congo red dye, New J. Chem. 35 (2011) 400–406.
[13] B. Jincheng Liu, H. Bai, Y. Wang, Z. Liu, X. Zhang, D.D. Sun, Self-assembling TiO_2 nanorods on large graphene oxide sheets at a two-phase interface and their anti-recombination in photocatalytic applications, Adv. Funct. Mater. 20 (2010) 4175–4181.
[14] M. Inagaki, Y.A. Kim, M. Endo, Graphene: preparation and structural perfection, J. Mater. Chem. 21 (2011) 3280–3294.
[15] N. Yang, J. Zhai, D. Wang, Y. Chen, L. Jiang, Two dimensional graphene bridges enhanced photoinduced charge transport in dye sensitized solar cells, ACS Nano 4 (2010) 887–894.
[16] P.V. Kamat, Graphene-based nanoarchitectures. Anchoring semiconductor and metal nanoparticles on a two-dimensional carbon support, J. Phys. Chem. Lett. 1 (2010) 520–527.
[17] O. Akhavan, E. Ghaderi, Photocatalytic reduction of graphene oxide nanosheets on TiO_2 thin film for photoinactivation of bacteria in solar light irradiation, J. Phys. Chem. C 113 (2009) 20214–20220.
[18] Y. Li, Y. Wu, Coassembly of graphene oxide and nanowires for large-area nanowire alignment, J. Am. Chem. Soc. 131 (2009) 5851–5857.
[19] H. Zhang, X. Lv, Y. Li, Y. Wang, J. Li, P25-graphene composite as a high performance photocatalyst, ACS Nano 4 (2010) 380–386.
[20] Z. Yong, B. Qiaoliang, A.L.T. Lena, Z. Yulin, L. Kian Ping, Hydrothermal dehydration for the "Green" reduction of exfoliated graphene oxide to graphene and demonstration of tunable optical limiting properties, Chem. Mater. 21 (2009) 2950–2956.
[21] Y. Zhou, Q. Bao, L.A.L. Tang, Y. Zhong, K.P. Loh, Chem. Mater. 21 (2009) 2950–2956.
[22] B. Zhao, B. Shi, X. Zhang, X. Cao, Y. Zhang, Catalytic wet hydrogen peroxide oxidation of H-acid in aqueous solution with TiO_2–CeO_2 and Fe/TiO_2–CeO_2 catalysts, Desalination 268 (2011) 55–59.
[23] F. Galindo-Hernandez, R. Gomez, Degradation of the herbicide 2,4-dichlorophenoxyacetic acid over TiO_2–CeO_2 sol–gel photocatalysts: effect of the annealing temperature on the photoactivity, J. Photochem. Photobiol. A: Chem. 217 (2011) 383–388.
[24] X. Gao, Y. Jiang, Y. Fu, Y. Zhong, Z. Luo, K. Cen, Preparation and characterization of CeO_2/TiO_2 catalysts for selective catalytic reduction of NO with NH_3, Catal. Commun. 11 (2010) 465–469.
[25] Z. Qiong, H. Yun Qiu, C. Xiao Gang, H. Dong Hu, L. Lin Jiang, Y. Ting, J. Ling Li, Structure and photocatalytic properties of TiO_2-graphene oxide intercalated composite, Chin. Sci. Bull. 56 (2011) 331–339.
[26] H. Lipson, H. Steeple, Interpretation of X-ray Powder Diffraction Patterns, Macmillan, London, 1970, p. 261.
[27] J. Zhang, Z. Xiong, X.S. Zhao, Graphene–metal–oxide composites for the degradation of dyes under visible light irradiation, J. Mater. Chem. 21 (2011) 3634–3640.

[28] J. Shen, B. Yan, M. Shi, H. Ma, N. Li, M. Ye, One step hydrothermal synthesis of TiO_2-reduced graphene oxide sheets, J. Mater. Chem. 21 (2011) 3415–3421.
[29] W. Fan, Q. Lai, Q. Zhang, Y. Wang, Nanocomposites of TiO_2 and reduced graphene oxide as efficient photocatalysts for hydrogen evolution, J. Phys. Chem. C 115 (2011) 10694–10701.
[30] A. Cao, R. Lu, G. Veser, Stabilizing metal nanoparticles for heterogeneous catalysis, Phys. Chem. Chem. Phys. 12 (2010) 13499–13510.
[31] H. Yang, K. Zhang, R. Shi, Sol–gel synthesis and photocatalytic activity of CeO_2/TiO_2 nanocomposites, J. Am. Ceram. Soc. 90 (2007) 1370–1374.
[32] G. Li, D. Zhang, J.C. Yu, Thermally stable ordered mesoporous CeO_2/TiO_2 visible-light photocatalysts, Phys. Chem. Chem. Phys. 11 (2009) 3775–3782.
[33] X.Y. Zhang, H.P. Li, X.L. Cui, Y. Lin, Graphene/TiO_2 nanocomposites: synthesis, characterization and application in hydrogen evolution from water photocatalytic splitting, J. Mater. Chem. 20 (2010) 2801–2806.
[34] C. Chen, W. Cai, M. Long, B.E. Zhou, Y. Wu, D. Wu, Y. Feng, Synthesis of visible-light responsive graphene oxide/TiO_2 composites with p/n heterojunction, ACS Nano 4 (2010) 6425–6432.
[35] R. Leary, A. Westwood, Carbonaceous nanomaterials for the enhancement of TiO_2 photocatalysis, Carbon 49 (2011) 741–772.
[36] G. Jiang, Z. Lin, C. Chen, L. Zhu, Q. Chang, N. Wang, W. Wei, H. Tang, TiO_2 nanoparticles assembled on graphene oxide nanosheets with high photocatalytic activity for removal of pollutants, Carbon 49 (2011) 2693–2701.
[37] Y. Zhang, C. Pan, TiO_2/graphene composite from thermal reaction of graphene oxide and its photocatalytic activity in visible light, J. Mater. Sci. 46 (2011) 2622–2626.